Integrated ligand and structure-based investigation of structural requirements for silent information regulator [SIRT1] activation

Amit K. Gupta[1], and Sun Choi[1*]

[1]National Leading Research Laboratory of Molecular Modeling & Drug Design, College of Pharmacy and Graduate School of Pharmaceutical Sciences, and Global Top 5 Research Program, Ewha Womans University, Seoul 03760, Republic of Korea.

Emails: (SC) sunchoi@ewha.ac.kr

Abstract.

A series of imidazothiazole and oxazolopyridine derivatives as human silent information regulator (SIRT1) activators were subjected to the integrated 2D and 3D QSAR approaches. The derived 3D QSAR models yielded high cross validated q^2 values of 0.682 and 0.628 for CoMFA and CoMSIA respectively. The non-cross validated values of $r^2_{training}$ = 0.89; predictive r^2_{test} = 0.69 for CoMFA and r^2=0.87; predictive r^2_{test} =0.67 for CoMSIA reflected the statistical significance of the developed model. The steric, electrostatic, hydrophobic and hydrogen bond acceptor interactions have been found important in describing the variation in human SIRT1 activation. Further, 2D QSAR model for the same dataset yielded high statistical significance and derived 2D model's parameters corroborated with 3D model in terms of features. The developed model was also validated by the crystal structure of active conformation of SIRT1. Developed models may be useful for the identification of potential novel human SIRT1 activators as therapeutic agent.

Keywords: SIRT1 activators, imidazothiazole and oxazolopyridine derivatives, 3D QSAR, 2D QSAR, CoMFA and CoMSIA.

1. Introduction

Human analogues of yeast Silent information regulator (SIR) protein also known as Sirtuins (SIRT) belong to class III of histone de-acetylases family (HDACs) [1,2] These proteins are classified as SIRT 1-7 according to their sequence similarity and inherent requirement for nicotinamide adenine dinucleotide (NAD) in mammalian domain [3]. SIRTs are evolutionarily conserved enzymes that differ significantly from other classes of histone de-acetylases because of their specialized functions in metabolic pathways [4]. Mammalian SIRTs are known to affect numerous cellular functions Related to aging, apoptosis, inflammation and endocrine signaling [5]. All seven mammalian sirtuins express ubiquitously across different types of tissues and have been categorized under four classes of proteins: SIRT1–3 (class I), SIRT4 (class II), SIRT5 (class III), and SIRT6–7 (class IV) [3]. The therapeutic efficacy of human SIRT1 activation has been explored in several cardio-vascular diseases [6] modulation of mitochondrial biogenesis, metabolic rate, insulin sensitivity, glucose and lipid metabolism [7-11] and in several age-related diseases [15]. Cardiac specific over expression of SIRT1 has been known to prevent age-dependent increase in cardiac hypertrophy, apoptosis, cardiac dysfunction, and expression of senescence markers [6, 12]. SIRT's catalytic domain consists two sub-domains; a large NAD+ binding subdomain and a small Zn2+-binding subdomain module has been resolved [13, 14]. SIRT1 activation is believed to be largely regulated by its allosteric site [15–16].

Resveratrol, a natural SIRT1 activator has been shown to improve the metabolic state of rodent models of obesity and type-2 diabetes mellitus [7, 17]. The SIRT1 activators could be mainly categorized into two classes: natural plant polyphenols and synthesized small molecules which include imidazo[1,2-b]thiazole derivatives [18], oxazolo[4,5-b]pyridines and their related

heterocyclic analogs [19], 1,4-dihydropyridine analogs [20], resveratrol analogues [21, 22], and some quinoxaline analogs [23]. The crystal structure of human SIRT-1 protein with its small molecule activator was unknown until recently [24], thus few ligand-based studies have been reported on SIRT1 activators [25, 26]. However, no quantitative validation of the reported models has been reported in these studies. Our past successful efforts of integrated ligand- and structure-based drug discovery on other targets [27, 28, 29, 30] encouraged us to use this approach in the presented project. We herein report a ligand-based 3D QSAR models using known SIRT1 activators and its validation through available crystal structure of SIRT1.

2. Methodology

2.1. Dataset

The QSAR studies have been performed on a dataset of fifty compounds belonging to Imidazothiazole and Oxazolopyridine class having human SIRT1 activation potency with $EC_{1.5}$ values ranging from 0.16µM to 130µM [18, 19]. Activation in the assay was measured as the concentration of compound required to increase the enzyme activity by 50% ($EC_{1.5}$). The $EC_{1.5}$ values were converted into negative logarithm of $EC_{1.5}$ ($pEC_{1.5}$) for the use in the QSAR studies. The fifty compounds in the dataset were rationally distributed into a training set of 26 molecules and a test set of 24 molecules to generate the QSAR models and evaluate the predictive ability of the developed models respectively. The chemical structures along with their biological activity of all the dataset compounds have been shown in Figure1, Table1 and Table 2.

Please insert **Figure 1** about here.

Please insert **Table 1** about here.

Please insert **Table 2** about here.

2.2. Computational approach and Molecular alignment

The 3D-QSAR techniques such as CoMFA and CoMSIA have been widely used in computer-aided drug discovery to understand the mechanism of action of drug–receptor interaction and for designing potent inhibitors [31-32]. CoMFA and CoMSIA studies were performed using SYBYL molecular modeling software running on a Silicon Graphics Octane R12000 workstation [33]. Molecular structures of all the compounds were drawn using the most active compound **43** as a template in SYBYL where partial charges were calculated using Gasteiger-Hückel method and geometry optimized using Tripos force field with a distance-dependent dielectric function and energy convergence criterion of 0.001 kcal/mol Å using 1000 iterations and standard SYBYL settings. The conformational search was performed using multi-search method with the following settings: maximum cycles (400), maximum conformers (400), energy cutoff (70 kcal/mol), maximum rms gradient (3.0) tolerance (0.40), and number of hit (12). The minimum energy conformations thus obtained were used in the analysis. The core (shown in pink color) of the most active compound **43** (Figure 2A) was used as a template for molecular alignment and the calculated $pEC_{1.5}$ values were used as dependent variables for carrying out PLS analysis in CoMFA and CoMSIA study. The overall alignment of the training set molecules has been shown in Figure2B.

Please insert **Figure 2** about here.

2.3. CoMFA and CoMSIA model generation

2.3.1. CoMFA

Aligned molecules of the training set were positioned in a 3D cubic lattice with a grid spacing of 2.0 Å in x, y and z directions for deriving the CoMFA fields. Steric (Lennard–Jones potential) and electrostatic (Columbic with 1/r dielectric) fields were calculated at each lattice point using Tripos force field and a distance dependent dielectric constant of 1.0. A sp^3-hybridised carbon with a +1.0 charge and a radius of 1.52 Å was used as a probe to calculate various steric and electrostatic fields. An energy cutoff value of 30 kcal/mol was applied to avoid too high and unrealistic energy values inside the molecule.

2.3.2. CoMSIA

The CoMSIA technique is based on the molecular similarity indices with the same lattice box used for the CoMFA calculations [29]. It is considered superior to CoMFA technique in certain aspects such as the results remain unaffected to both, region shifts as well as small shifts within the alignments, it does not require steric cutoffs and more intuitively interpretable contour maps. In the present study, five different similarity fields *viz.* steric, electrostatic, hydrophobic, H-donor and H-acceptor were calculated using the standard settings of CoMSIA (Probe with charge +1, radius 1 Å and hydrophobicity +1, hydrogen-bond donating +1, hydrogen-bond accepting +1, attenuation factor of 0.3 and grid spacing 2 Å).

2.3.3. Partial least squares (PLS) and Predictive r_2 analysis

PLS is used to correlate SIRT1 activity with the CoMFA and CoMSIA values containing magnitude of steric, electrostatic and hydrophobic potentials. Leave one out (LOO) validation was utilized as tool for determining the predictability of the developed model. In addition to LOO cross validation a group cross validation using 20 groups, repeating the procedure 20 times

was also carried out. The mean of 20 readings is given as $r^2_{cv(mean)}$. The full PLS analysis was carried out with a column filtering of 2.0 kcal/mol to speed up the calculation and reduce the noise. To further assess the robustness and statistical confidence of the derived models, bootstrapping analysis (20 runs) was also performed. The predictive r^2 value is based on the only test set molecules which may be define as

$$r^2 (pred) = \frac{(SD - PRESS)}{SD}$$

where SD is the sum of squared deviation between the biological activities of the test set molecule to the mean activity of the training set molecules while PRESS is the sum of squared deviations between the observed and the predicted activities of the test molecules [30].

2.4. 2D QSAR model generation

In *2D QSAR* analysis constitutional, topological descriptors, BCUT, geometrical descriptors were calculated using PaDEL-Descriptor software [34]. Linear regression was performed using Systat (v12.2) software using the SIRT1 $pEC_{1.5}$ as dependent and ligand-based physicochemical parameters as independent parameters. Pearson correlation matrix was constructed to determine the inter-correlation between the independent parameters and the correlation between the dependent and independent parameters. Stepwise multi-parameter regression analysis was performed by backward elimination method using Systat software (v12.2). These descriptors were then used to generate an equation which would give insight into the various physicochemical and structural parameters influencing SIRT1 activation.

2.5. Molecular docking

The SIRT1 protein structure (PDB ID: 4ZZH) was prepared for docking using the protein preparation wizard of the Schrodinger Suite of programs (Small molecule drug discovery suite2015-2, S., LLC, NY. 2015) with default options to assign bond order and remove water molecules that are 5 Å away from hetero groups. H-bond assignment was done using PROPKA at pH 7.0 and the orientation of hydroxyl groups, amide groups of Asn and Gln, and charge state of His residues were optimized. At the end, protein was minimized to an RMSD limit from the starting structure of 0.3 Å with the OPLS3 force field. Binding site/docking grid was defined by selecting co-crystallized small molecule SIRT1 activator. The ligand libraries were prepared using LigPrep with Epik at pH 7.0 while retaining specific chirality of the ligands. Partial atomic charges were computed using the OPLS-3 force field and lowest energy conformation was retained. The lowest energy conformation among the largest populated cluster sharing common interactions was selected as the best binding pose for docked ligands.

3. Results and discussion

CoMFA and CoMSIA techniques were used to derive 3D-QSAR models on a set of 50 chemically diverse human SIRT1 activators. Among the various 3D-QSAR models were generated and the best one was selected based on the statistically significant parameters obtained. The predictive power of the generated 3D-QSAR models, was assessed by predicting biological activities of the test set molecules. The results of the CoMFA, CoMSIA studies have been summarized in Table 3.

Please insert **Table 3** about here.

3.1. CoMFA analysis

The CoMFA analysis revealed a cross validated q^2 of 0.682 for 2 principal components and a non-cross validated conventional r^2 of 0.889, F value of 100.56 and standard error of estimate SEE of 0.247. To further assess the robustness of this model, bootstrapping analysis (20 runs) was performed to give r^2_{bs} of 0.931 (SD_{bs} = 0.029) thus establishing the strength of the model. In addition to LOO, a group cross validation was further done to assess the internal predictive ability of the model. The cross-validation for 20 times was performed with 20 groups and the mean r^2_{CV} of 0.670 (TS) revealed that the model has good internal predictability and the results have no chance correlation (Table 3). A test set of 24 molecules was used to evaluate the predictivity of the generated model and a predictive r^2 of 0.694 showed good predictive ability of the generated model (Figure 3A). The Predictive $pEC_{1.5}$ values of the training as well as test set molecules based on the CoMFA model have been included in the Table 1 and Table 2 respectively.

Please insert **Figure 3** about here.

3.2. CoMSIA analysis

The CoMSIA model having steric(S), electrostatic (E), hydrophobic (H) and hydrogen bond acceptor (A) descriptors gave the highest q^2 value of 0.628 at 2 components and a conventional non cross-validated r^2 of 0.870, F value of 83.94 and standard error of estimate SEE of 0.267. To further assess the statistical ability and robustness of the model, bootstrapping analysis (20 runs) was performed where r^2_{bs} of 0.917 with low standard deviation of 0.020 were obtained thus showing the robustness of the model. Like CoMFA, internal predictive ability of the model was accessed by group cross-validation performed with 20 groups. The mean r^2_{cv} value of 0.625

revealed that the model has high internal predictivity. Further predictive r^2 of 0.666 for the 24 test set compounds showed the usefulness of the model (Figure 3B). The Predictive $pEC_{1.5}$ values of the training as well as test set molecules based on the CoMSIA model have been included in the Table1 and Table 2 respectively.

3.3. CoMFA and CoMSIA contour maps analysis

The coefficients from CoMFA and CoMSIA models were used to generate 3D contour maps. These contours indicate regions in 3D space around the dataset molecules where changes in the physicochemical properties are predicted to vary the biological potency. A thorough analysis of the contours obtained determines the vital physicochemical properties responsible in determining the activity and explores the crucial importance of various substituents in their 3D orientation. The Contour maps generated from the above hypothesis of CoMFA and CoMSIA analyses are shown in Figure 4.

Please insert **Figure 4** about here.

A contrast of the contours obtained from the PLS co-efficient of CoMFA and CoMSIA descriptors yields necessary information about the physicochemical properties of the molecules vital in defining the potency of a chemical moiety in activating human SIRT1. An analysis of the CoMFA and CoMSIA contours around the most active molecule of the dataset **43** signify the importance of sterically favorable region (green color) near the 6, 7, 8 position of quinoxaline moiety for SIRT1 activation. The higher activities among all the active compounds of the training set (viz. compound **43, 13, 50, 15, 14, 27, 41, 46, 44, 5** and **9**) can be explained based on presence of aromatic ring of the quinoxaline moiety at the same position. It has been also found

that an addition of bulky group near 29, and 30 positions of the piperazine moiety further increased the SIRT1 activation potency (*viz.* compound **43, 14, 41, 46, 44, 5** and **42**). The absence of such functionality in 3D space led to the decrease in the activation potency (viz. compound **2, 25, 32, 3, 35, 1,** and **31**). The sterically unfavorable region at the upper side of the 4, 5 positions of quinoxaline ring as well as on the lower plane of the piperazine moiety has been found important for SIRT 1 activation (Figure 4A).

When the electrostatic contours were considered, both the CoMFA and CoMSIA contours emphasized the importance of the electropositive substituent near the amide moeity and the presence of substituent with high electronegative functionality in the region adjoining the nitrogen atom at the 9 positions to the keto oxygen of the quinoxaline ring, for high SIRT1 activation potency. These contours also conclude the fact that optimal activation potency is achieved when the electronegative functionality at that region is being contributed by the nitrogen atom (Figure 4A and 4B).

The PLS contour analysis of the hydrogen bond acceptor feature highlighted the importance of the presence of a hydrogen bond acceptor atom in the vicinity of the ketonic oxygen atom at position 9 of the molecule. These contours well explain the variation in biological activity among the compounds of series (compounds **1, 2, 3, 25, 31,** and **35** failed to map the H-bond acceptor group at this 3D space represent least potent molecules of this series). The space present in between and behind the phenyl ring and the piperazine ring has been found unfavorable for acceptor functionality (Figure 4C). In the case of hydrophobic contours, the hydrophobic favorable regions near the 5 position of quinoxaline ring and around piperazine nucleus while

hydrophobic disfavored regions around the CONH functionality of the molecule **43** facilitate the effective binding of SIRT1 activators to the target protein (Figure 4C).

3.4. 2D QSAR Analysis

CoMFA and CoMSIA predictive models can be sensitive to ligand alignment [35]. Therefore, to rule out any false positive results, and validate the model we performed alignment free 2D QSAR analysis for the same dataset. Different combination of physiochemical parameters showing some acceptable correlation with the biological activity were carried out using stepwise multiple regression analysis to develop meaningful QSAR equations.

We derived structure activity relationship equation for all the 50 dataset ligands. The generated equation showed the importance of Polarizability (AMR) [36], BCUT (SPMAX3_BHS) [37] and topological parameter (WPOL) [38] in defining the structure activity relationship of SIRT1 activators. Regression analysis of the above physico-chemical parameters with biological activity generated following equation:

$pE.C_{1.5}$ = -7.96(±1.58) - 0.038(±0.006)*AMR + 1.224(±0.418)*SPMAX3_BHS + 0.091 (±0.014)*WPOL ------ (Eq. 1)

n=49; r= 0.751; r^2= 0.564; r^2_{adj}= 0.535; SE=0.436; F=19.43; df=3

Eq. 1 showed 99.99% significance with the correlation coefficient value of 0.75 between the predicted and observed activity (Figure 5) after removal of one outlier compound (Compound **45**). The low standard error of estimate(s) and a high F value suggests that the model is highly

statistically significant. Values of physico-chemical parameters used in the equations as well as observed and predicted activities of all compounds in training and test set listed in Table 4.

Please insert **Table 4** about here.

Table 5 lists the Pearson Correlation Matrix of the significant parameters used in the equation.

Please insert **Table 5** about here.

The correlation between observed and predicted activities of all compounds using Eq. 1 has been represented graphically as shown in Figure 5.

Please insert **Figure 5** about here.

Significant contribution of lipophilicity (AMR) parameter suggests the role of hydrophobic and van-der-Waals interactions in defining the variation in the biological activity of SIRT1 activators. Further, contribution of BCUT (SPMAX3_BHS) and topological parameter (WPOL) suggests the importance of hydrogen bonds, charge transfer interactions and steric hindrance geometric fit for SIRT-1 activation. These features are consistent with our 3D CoMFA and CoMSIA model where importance of all these features has been well explained.

3.5. Structure based validation of CoMFA, CoMSIA model

A recently reported structure of SIRT1-enzyme-activator complex [24] enabled us to validate our CoMFA, CoMSIA model. Figure 6 represents lowest energy conformation of most active compound bound with active form of SIRT1. Quinoxaline moiety of compound **43** has made hydrophobic contact with Ile227 and Ile223 at its 4, 5, 6 position which corroborated with

hydrophobically favored cotutors of CoMFA and CoMSIA. Interaction of small molecule with Glu230 is very critical for SIRT1 activation. Glu230 also plays pivotal role of an electrostatic interaction between Glu230 and Arg446 in the activated conformation. Presence of any bulkier group will negatively impact the SIRT1 activation as shown in hydrophobic unfavorable contours of Figure 4. The Nitrogen atom of piperazine ring of compound **43** makes the H-bond interaction with Glu230 (Figure 6) well captured by electronegative contours in Figure 4. Other H-bond interactions between amide bond of compound **43** and residue Asn226, and Ile223 were well predicted by H-bond contours of CoMSIA model. In summary, our CoMFA, CoMSIA models predict the binding site interactions of small molecule SIRT1 activators very well.

Please insert **Figure 6** about here.

4. Conclusion

The CoMFA and CoMSIA have been applied successfully to rationalize the structurally diverse SIRT1 activators. Structural features in terms of their steric, electrostatic, hydrophobic and hydrogen bond acceptor interactions in 3D space have been found important. The developed 3D models showed good statistical significance in internal validation (q^2, group cross-validation and bootstrapping) and performed very well in predicting the SIRT 1 activation by the compounds in the test set. The developed model was also validated by 2D QSAR model as well as the crystal structure of active conformation of SIRT1. These models alone or in combination may be useful in the designing novel human SIRT1 activators with increased potency.

Acknowledgement

This work was supported by the Mid-career Researcher Program (NRF-2017R1A2B4010084), Bio & Medical Technology Development Program (No. 2018M3A9A7057263), and Medical Research Center (MRC) grant (No. 2018R1A5A2025286) funded by the Ministry of Science and ICT (MSIT) through the National Research Foundation of Korea (NRF).

The authors declare no conflict of interests.

References

[1] Blander, G.; Guarente, L. The Sir2 family of protein deacetylases. *Annu. Rev. Biochem*, **2004**, 73, 417-435.

[2] Khochbin, S.; Verdel, A.; Lemercier, C.; Seigneurin-Berny, D. Functional significance of histone deacetylase diversity. *Curr. Opin. Genet. Dev.* **2001**, 11, 162-166.

[3] Schwer, B.; Verdin, E. Conserved metabolic regulatory functions of sirtuins. Cell Metab. 2008, 7, 104-112.

[4] Gregoretti, I.V.; Lee, Y.M.; Goodson, H.V. Molecular evolution of the histone deacetylase family: functional implications of phylogenetic analysis. *J. Mol. Biol.* **2004**, 338, 17-31.

[5] Preyat, N.; Leo, O. Sirtuin deacylases: a molecular link between metabolism and immunity. *J. Leukoc. Biol*. **2013**, 93, 669–680.

[6] Matsushima, S.; Sadoshima, J. The role of sirtuins in cardiac disease. *Am. J. Physiol. Heart Circ. Physiol.* **2015** 309(9), H1375–H1389.

[7] Mattagajasingh, I.; Kim, C.S.; Naqvi, A.; Yamamori, T.; Hoffman, T.A.; Jung, S.B.; DeRicco, J.; Kasuno, K.; Irani, K. SIRT1 promotes endothelium-dependent vascular relaxation by activating endothelial nitric oxide synthase. *Proc. Natl. Acad. Sci.* **2007**, 104, 14855-14860.

[8] Potente, M.; Ghaeni, L.; Baldessari, D.; Mostoslavsky, R.; Rossig, L.; Dequiedt, F.; Haendeler, J.; Mione, M.; Dejana, E. SIRT1 controls endothelial angiogenic functions during vascular growth. *Genes Dev.* **2007**, 21, 2644-2658.

[9] Li, X.; Zhang, S.; Blander, G.; Tse, J.G.; Krieger, M.; Guarente, L. SIRT1 deacetylates and positively regulates the nuclear receptor LXR. *Mol. Cell* **2007**, 28, 91-106.

[10] Lagouge, M. ; Argmann, C. ; Gerhart-Hines Z. ; Meziane, H. ; Lerin, C. ; Daussin, F. ; Messadeq, N. ; Milne, J. Lambert, P. ; Elliott, P. ; Geny, B. ; Laakso, M. ; Puigserver, P. ; Auwerx, J. Resveratrol improves mitochondrial function and protects against metabolic disease by activating SIRT1 and PGC-1alpha, *Cell* **2006**, 127, 1109–1122.

[11] Milne, J.C.; Lambert, P.D.; Schenk, S.; Carney, D.P.; Smith, J.J.; Gagne, D.J.; Jin, L.; Boss, O.; Perni, R.B.; Vu, C.B.; Bemis, J. E.; Xie, R.; Disch, J.S.; Ng, P.Y.; Nunes, J.J.; Lynch, A.V.; Yang, H.; Galonek, H.; Israelian, K.; Choy, W.; Iffland, A.; Lavu, S.; Medvedik, O.; Sinclair, D.A.; Olefsky, J.M.; Jirousek, M.R.; Elliott, P.J.; Westphal, C.H. Small molecule activators of SIRT1 as therapeutics for the treatment of type 2 diabetes, Nature **2007**, 450, 712–716.

[12] Yamamoto, H.; Schoonjans, K.; Auwerx, J. Sirtuin functions in health and disease, *Mol. Endocrinol.* **2007**, 21, 1745–1755.

[13] Zhao, X.; Allison, D.; Condon, B.; Zhang, F.; Gheyi, T.; Zhang, A.; Ashok, M.; MacEwan, R.I.; Qian, Y.; Jamison, J.A.; Luz, J.G. The 2.5 Å crystal structure of the SIRT1 catalytic domain bound to nicotinamide adenine dinucleotide (NAD+) and an indole (EX527 analogue) reveals a novel mechanism of histone deacetylase inhibition, *J. Med. Chem.* 2013,14, 963–969.

[14] Davenport, A.M.; Huber, F.M.; Hoelz, A. Structural and functional analysis of human SIRT1, *J. Mol. Biol.* **2014**, 426, 526–541.

[15] Autiero, I.; Costantini, S.; Colonna, G. Human sirt-1: molecular modeling and structure-function relationships of an unordered protein, *PLoS One* **2009**, 4, e7350.

[16] Sharma, A.; Gautam, V.; Costantini, S.; Paladino, A.; Colonna, G. Interactomic and pharmacological insights on human Sirt-1, *Front. Pharmacol.* **2012**, 3, 40.

[17] Baur, J. A.; Pearson, K.J. ; Price, N.L. ; Jamieson, H.A. ; Lerin, C. ; Kalra, A. Prabhu, V.V. ; Allard, J. S. ; Lopez-Lluch, G. ; Lewis, K.; Pistell, P.J. ; Poosala, S.; Becker, K.G.; Boss, O. ; Gwinn, D. ; Wang, M. ; Ramaswamy, S.; Fishbein, K.W. ; Spencer, R.G. ; Lakatta, E.G. ; Le Couteur, D. ; Shaw, R.J. ; Navas, P. ; Puigserver, P. ; Ingram, D.K. ; de Cabo, R. ; Sinclair, D.A. Resveratrol improves health and survival of mice on a high-calorie diet. *Nature* **2006**, 444, 337–342.

[18] Vu, C.B.; Bemis, J.E.; Disch, J.S.; Ng, P.Y.; Nunes, J.J.; Milne, J.C.; Carney, D.P.; Lynch, A.V.; Smith, J.J.; Lavu, S.; Lambert, P.D.; Gagne, D.J.; Jirousek, M.R.; Schenk, S.; Olefsky, J.M.; Perni, R.B. Discovery of imidazo[1,2-b]thiazole derivatives as novel SIRT1 activators. *J. Med. Chem.* **2009**, 52, 1275–1283.

[19] Bemis, J. E.; Vu, C.B.; Xie, R.; Nunes, J. J.; Ng, P.Y.; Disch, J.S.; Milne, J.C.; Carney, D.P.; Lynch, A.V.; Jin, L.; Smith, J.J.; Lavu, S.; Iffland, A.; Jirousek, M.R.; Perni, R.B. Discovery of oxazolo[4,5-b] pyridines and related heterocyclic analogs as novel SIRT1 activators. *Bioorg. Med. Chem. Lett.* **2009**, 19, 2350–2353.

[20] Mai, A. ; Valente, S. ; Meade, S. ; Carafa, V. ; Tardugno, M.; Nebbioso, A. ; Galmozzi, A. ; Mitro, N. ; Fabiani, E.D. ;. Altucci, L.; Kazantsev, A. Study of 1,4-dihydropyridine structural scaffold: discovery of novel sirtuin activators and inhibitors. *J. Med. Chem.* **2009**, 52, 5496–5504.

[21] Howitz, K.T.; Zipkin, R.E. Compositions and methods for selectively activating human sirtuins. **2006**, US20060014705A1.

[22] Milburn, M.; Milne, J.; Auwerx, J.; Argmann, C.; Lagouge, M.; Dipp, M. Methods and related compositions for treating or preventing obesity, insulin resistance disorders, and mitochondrial-associated disorders, **2007**, US20070149466A1.

[23] Nayagam, V.M.; Wang, X.; Tan, Y.C.; Poulsen, A.; Goh, K.C.; Ng, T.; Wang, H.; Song, H.Y.; Ni, B.; Entzeroth, M. SIRT1 modulating compounds from high-throughput screening as anti-inflammatory and insulin-sensitizing agents. *J. Biomol. Screen.* **2006**, 11, 959-967.

[24] Dai, H.; Case, A.W.; Riera, T.V.; Considine, T.; Lee, J.E.; Hamuro, Y.; Zhao, H.; Jiang, Y.; Sweitzer, S.M.; Pietrak, B.; Schwartz, B.; Blum, C.A.; Disch, J.S.; Caldwell, R.; Szczepankiewicz, B.; Oalmann, C.; Yee, Ng P.; White, B.H.; Casaubon, R.; Narayan, R.; Koppetsch, K.; Bourbonais, F.; Wu, B.; Wang, J.; Qian, D.; Jiang, F.; Mao, C.; Wang, M.; Hu, E.; Wu, J.C.; Perni, R.B.; Vlasuk, G.P.; Ellis, J.L. Crystallographic structure of a small molecule SIRT1 activator-enzyme complex. *Nat. commun.*, **2015**. 6, 7645.

[25] Sakkiah, S.; Arooj, M.; Lee, K.W.; Torres, J.Z. Theoretical approaches to identify the potent scaffold for human sirtuin1 activator: Bayesian modeling and density functional theory. *Med. Chem. Res.*, **2014**, 23, 3998–4010.

[26] Vyas, V.K.; Goel, A.; Ghate, M.; Patel, P., Ligand and structure-based approaches for the identification of SIRT1 activators, *Chem. Biol. Interact*. **2015**, 228, 9–17.

[27] Gupta, A.K.; Bhunia, S.S., Balaramnavar, V.M.; Saxena, A.K. Pharmacophore modelling, molecular docking and virtual screening for EGFR (HER 1) tyrosine kinase inhibitors, SAR QSAR Env. Res. **2011**, 22, 239-263.

[28] Gupta, A.K.; Saxena, S.; Saxena, M. Integrated ligand and structure-based studies of flavonoids as fatty acid biosynthesis inhibitors of Plasmodium falciparum, *Bioorg. Med. Chem. Lett.* **2010**, 20, 4779–4781.

[29] Gupta, A.K.; Varshney, K.; Saxena, A.K. Toward the Identification of a Reliable 3D QSAR pharmacophore Model for the CCK2 Receptor Antagonism. *J. Chem. Inf. Model.* **2012**, 52, 1376–1390.

[30] Khare, P.; Gupta, A.K.; Gajula, P.K.; Sunkari, K.Y., Jaiswal, A.K.; Das, S.; Bajpai, P., Chakraborty TK, Dube A, Saxena AK. Identification of novel s-adenosyl-l-homocysteine hydrolase inhibitors through homology-model-based virtual screening, synthesis, and biological evaluation, *J. Chem. Inf. Model.* **2012**, 52, 777-779.

[31] Gupta, A.K.; Saxena, A.K. 3D-QSAR CoMFA and CoMSIA studies on a set of diverse α -adrenergic receptor antagonists. *Med. Chem. Res.* **2011**, 20, 1455-1464.

[32] Gupta, A.K.; Saxena, A.K. Triple-layered QSAR studies on substituted 1,2,4-trioxanes as potential antimalarial agents: superiority of the quantitative pharmacophore-based

alignment over common substructure-based alignment, *SAR QSAR Env. Res.* **2013**, 24, 119-134.

[33] SYBYL 6.9, Tripos Inc., South Hanley Road, St. Louis, MO 63144, 1699.

[34] Gohda, K.; Mori, I.; Ohta, D.; Kikuchi, T.A.; CoMFA analysis with conformational propensity: an attempt to analyze the SAR of a set of molecules with different conformational flexibility using a 3D-QSAR method. *J. Comput. Aided Mol. Des.* **2000**, 14, 265–275.

[35] Yap, C.W.; PaDEL-Descriptor: An open source software to calculate molecular descriptors and fingerprints. *J. Comp. Chem.* 2011, 32, 1466-1474.

[36] Wildman, S.A.; Crippen, G.M. Prediction of Physicochemical Parameters by Atomic Contributions. *J. Chem. Inf. Comput. Sci.* **1999**, 39, 868-873.

[37] Todeschini, R.; Consonni, V. Molecular descriptors for chemoinformatics. Weinheim: Wiley VCH, 2009, 714-726.

[38] Wiener and Harry, Structural Determination of Paraffin Boiling Points, J. Am. Chem. Soc., 69(1947), pp. 17-20.

Table 1. Structures of the training set compounds along with their experimental and predicted biological activity.

Comp. Name	R_1	R_2	ALog P	Experimental $EC_{1.5}$ Activity (µM)	Experimental $pEC_{1.5}$ (µM)	Predictive CoMFA $pEC_{1.5}$	Predictive CoMSIA $pEC_{1.5}$
1	-	-	3.014	46	-1.66	-1.178	-1.218
2	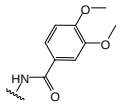	H	2.9414	6	-0.78	-1.102	-1.093
3	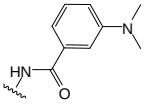	H	3.1364	25	-1.4	-1.288	-1.246
4	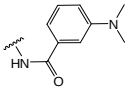	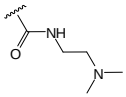	2.4832	1.8	-0.26	-0.058	0.06
5	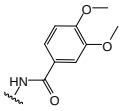	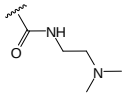	2.2882	0.7	0.15	0.227	0.303
6	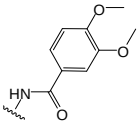		3.015	1.1	-0.04	0.099	0.089
7	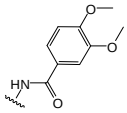	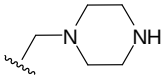	2.4364	1.1	-0.04	0.189	0.118
9	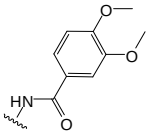	H	2.9414	0.9	0.05	-0.102	-0.34
10	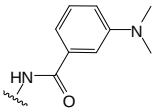	H	3.1364	4.4	-0.64	-0.482	-0.444
11	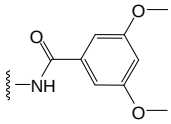	H	3.689	1.7	-0.23	-0.14	-0.29

13	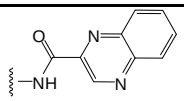	H	3.6145	0.3	0.52	0.31	0.327
14	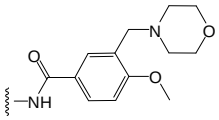	H	3.4667	0.5	0.3	0.301	0.352
15	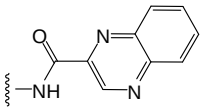	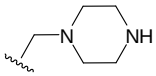	3.1095	0.4	0.4	0.443	0.461
21	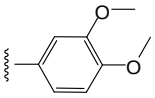	-	2.643	1.4	-0.15	-0.04	-0.103
25	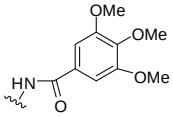	H	3.2289	7.5	-0.88	-1.249	-1.355
26	H	H	3.2289	2.5	-0.4	-0.394	-0.353
29	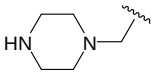	H	2.939	3.2	-0.51	-0.61	-0.38
31		-	2.9941	130	-2.11	-1.759	-1.831
32	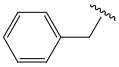	-	3.023	14	-1.15	-0.935	-0.705
35	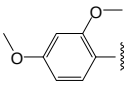	-	2.9554	31	-1.42	-1.785	-1.729
37	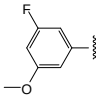	-	3.1773	2.1	-0.32	-0.588	-0.596
39	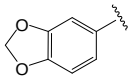	-	2.7563	4.9	-0.69	-0.596	-0.496
41	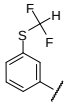	-	4.3519	0.51	0.29	-0.018	-0.025
42	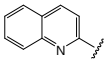	-	3.603	0.99	0	0.307	0.271

43	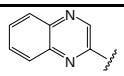	-	2.8809	0.16	0.8	0.465	0.547
44	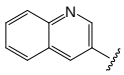	-	3.1745	0.68	0.17	0.311	0.097
46	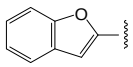	-	3.4928	0.61	0.21	0.202	0.099
50		H	3.2618	0.4	0.4	0.099	0.11

Table 2. Structures of the test set compounds along with their experimental and predicted biological activity.

Comp. Name	R_1	R_2	ALog P	Experimental $EC_{1.5}$ Activity (μM)	Experimental $pEC_{1.5}$ (μM)	Predictive CoMFA $pEC_{1.5}$	Predictive CoMSIA $pEC_{1.5}$
8	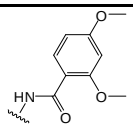	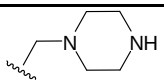	2.4364	0.5	0.3	0.141	0.294
12	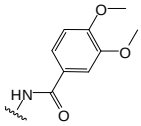	H	3.689	0.4	0.4	0.174	0.015
16	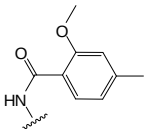	-	3.1456	4.1	-0.61	-0.46	-0.515
17	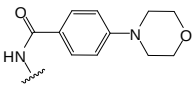	-	2.5257	0.9	0.05	-0.022	-0.3
18	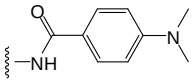	-	2.838	0.7	0.15	-0.043	-0.329
19	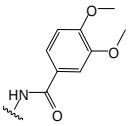	-	2.643	0.5	0.3	-0.161	-0.286
20	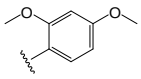	-	2.643	0.5	0.3	-0.059	-0.137
22	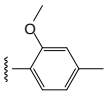	-	3.1456	2.3	-0.36	-0.333	-0.271
23	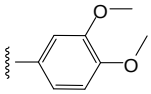	-	2.643	1.6	-0.2	-0.259	-0.056

24	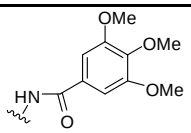	H	2.925	11	-1.04	-1.109	-1.226
27	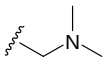	H	3.5176	4.8	-0.68	-0.616	-0.365
28	H		3.5176	1.9	-0.28	-0.089	-0.185
30	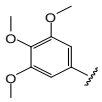	-	2.939	1.8	-0.26	-0.03	-0.21
33	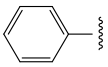	-	2.9882	25	-1.4	-1.601	-1.532
34	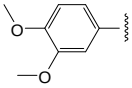	-	2.9554	4.5	-0.65	-0.616	-0.616
36	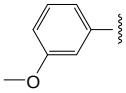	-	2.9718	3.7	-0.57	-0.578	-0.608
38	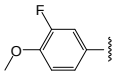	-	3.1773	6.2	-0.79	-0.743	-0.673
40	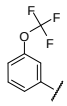	-	5.1081	0.90	0.05	-0.129	-0.08
45		-	3.1745	45	-1.65	-1.702	-1.769
47	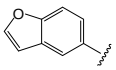	-	3.0643	6.9	-0.84	-1.618	-1.575
48	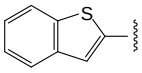	-	4.051	24	-1.38	-0.313	-0.46
49		-	1.1155	1.7	-0.23	-0.21	-0.429

Table. 3. PLS statistics of CoMFA (TS) and CoMSIA (SEHA) models.

Parameters		CoMFA (TS)	CoMSIA (SEHA)
q^2		0.682	0.628
PRESS		0.427	0.455
r^2		0.889	0. 870
SEE		0.247	0.267
F		100.557	83.939
N		2	2
Fractions	**S**	0.384	0.164
	E	0.616	0.320
	H	-	0.241
	A	-	0.276
r^2_{bs} (20runs)		0.931	0.917
SD_{bs}		0.029	0.020
$r^2_{CV\ (mean)}$ (20runs)		0.670	0.625
r^2_{pred}		0.694	0.666

q^2 = leave one out cross-validation correlation coefficient; PRESS = LOO cross-validated standard error / predictive sum of squares; r^2 = conventional correlation; SEE = standard error of estimate; F = degree of freedom; N = optimal number of component; r^2_{bs} = bootstrapping correlation; SD_{bs} = bootstrapping standard deviation; $r^2_{CV(mean)}$ = group cross-validation; TS = Tripos standard; SEHA = Steric, electrostatic, Hydrophobic and Acceptor.

Table 4. Values of descriptors used in the 2D QSAR equation as well as observed and predicted activities of all compounds in data set.

S.No.	Comp. name	AMR	SpMax3_Bhs	WPOL	Exp. $pEC_{1.5}$	Pred. $pEC_{1.5}$
1	1	18.0124	3.899546	21	-1.66	-1.96043
2	10	23.352	3.803955	42	-0.64	-0.36933
3	11	25.3731	3.840631	44	-0.23	-0.21925
4	12	25.3731	3.845228	45	0.4	-0.12262
5	13	10.7415	4.020921	45	0.52	0.648431
6	14	46.1354	3.869602	52	0.3	-0.24475
7	15	40.5005	4.07409	56	0.4	0.583667
8	16	23.5594	3.815775	43	-0.61	-0.27175
9	17	34.1074	3.847878	47	0.05	-0.26928
10	2	23.6922	3.849439	44	-0.78	-0.14459
11	18	25.0329	3.803657	42	0.15	-0.43357
12	19	25.3731	3.849434	45	0.3	-0.11747
13	20	25.3731	3.841818	44	0.3	-0.21779
14	21	25.3731	3.849438	44	-0.15	-0.20847
15	22	23.5594	3.815776	42	-0.36	-0.36275
16	23	25.3731	3.849439	44	-0.2	-0.20846
17	3	23.352	3.803842	41	-1.4	-0.46047

18	4	54.5093	4.204484	53	-0.26	-0.06206
19	5	54.8495	4.213282	56	0.15	0.208776
20	6	42.6958	3.860449	50	-0.04	-0.30725
21	7	53.4512	3.904407	55	-0.04	-0.20715
22	8	53.4512	3.896812	55	0.3	-0.21645
23	9	23.6922	3.849436	45	0.05	-0.05359
24	24	31.008	3.88292	49	-1.04	0.073391
25	27	59.084	3.888365	53	-0.68	-0.62283
26	28	59.084	3.888365	54	-0.28	-0.53183
27	29	69.8394	3.932994	58	-0.51	-0.52191
28	30	69.8394	3.932994	59	-0.26	-0.43091
29	31	66.2404	3.893735	42	-2.11	-1.8892
30	32	52.4412	3.865679	45	-1.15	-1.12617
31	33	47.892	3.821678	45	-1.4	-1.00716
32	25	40.0804	3.877184	46	-0.88	-0.55138
33	34	62.5236	3.901345	54	-0.65	-0.64665
34	35	62.5236	3.893742	54	-1.42	-0.65596
35	36	55.2078	3.859673	49	-0.57	-0.87466
36	37	56.0803	4.15223	51	-0.32	-0.36772
37	38	56.0803	4.15223	52	-0.79	-0.27672

38	39	55.3641	3.977493	51	-0.69	-0.55438
39	40	56.3188	4.562376	52	0.05	0.216234
40	41	61.388	4.55336	51	0.29	-0.07843
41	42	47.892	4.044413	54	0.0034	0.084466
42	43	47.892	4.076816	54	0.8	0.124127
43	26	40.0804	3.877176	47	-0.4	-0.46039
44	44	47.892	4.047861	54	0.17	0.088686
45	45	47.892	4.039226	55	-1.65	0.169116
46	46	49.5111	4.096784	51	0.21	-0.18596
47	47	49.5111	4.123483	51	-0.84	-0.15328
48	48	55.6855	3.969277	51	-1.38	-0.57665
49	49	47.892	3.909148	45	-0.23	-0.9001
50	50	47.2997	4.099622	53	0.4	0.083548

Table 5: Pearson Correlation Matrix of the significant parameters used in the equation.

	AMR	**SPMAX3_BHS**	**WPOL**
AMR	1.000		
SPMAX3_BHS	0.431	1	
WPOL	0.707	0.431	1.000

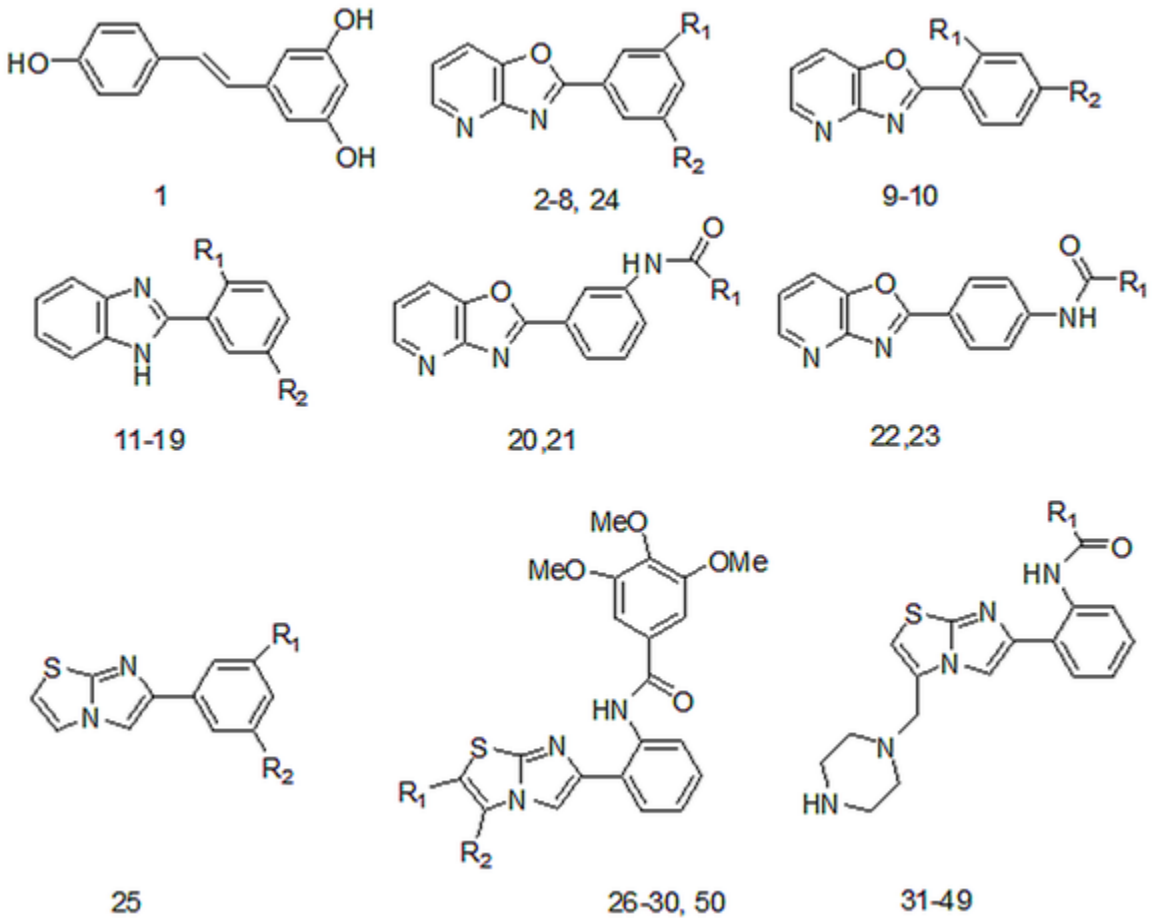

Figure 1. Common Structure of the SIRT1 activators used in the 3D-QSAR study.

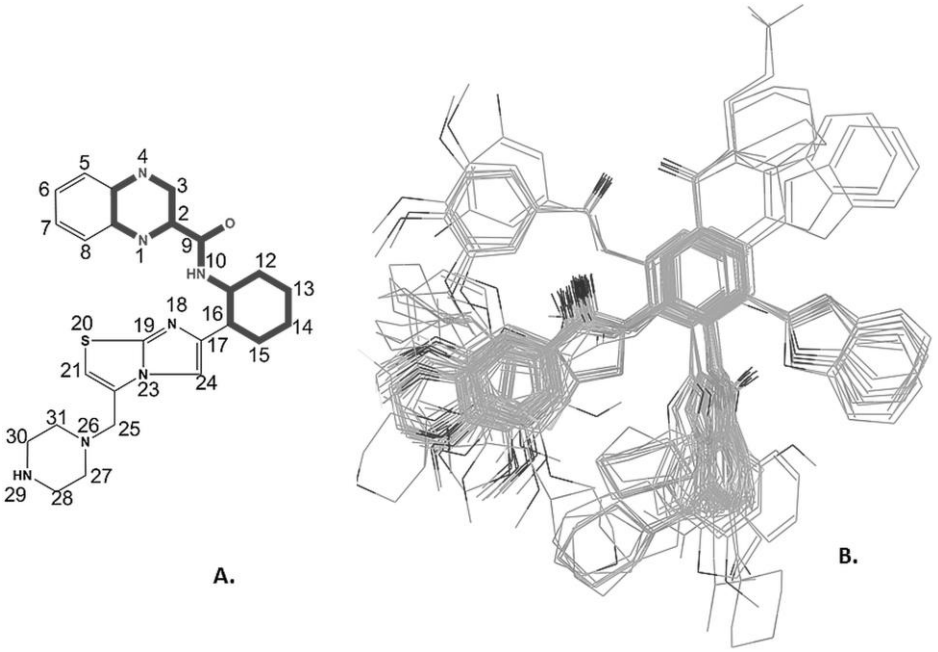

Figure 2. (A) The core structure (shown in bold) of the most active molecule of the dataset (compound **43**) and the numbering system used in the 3D-QSAR study. **(B)** The overall alignment of the training set molecules used in the 3D-QSAR study.

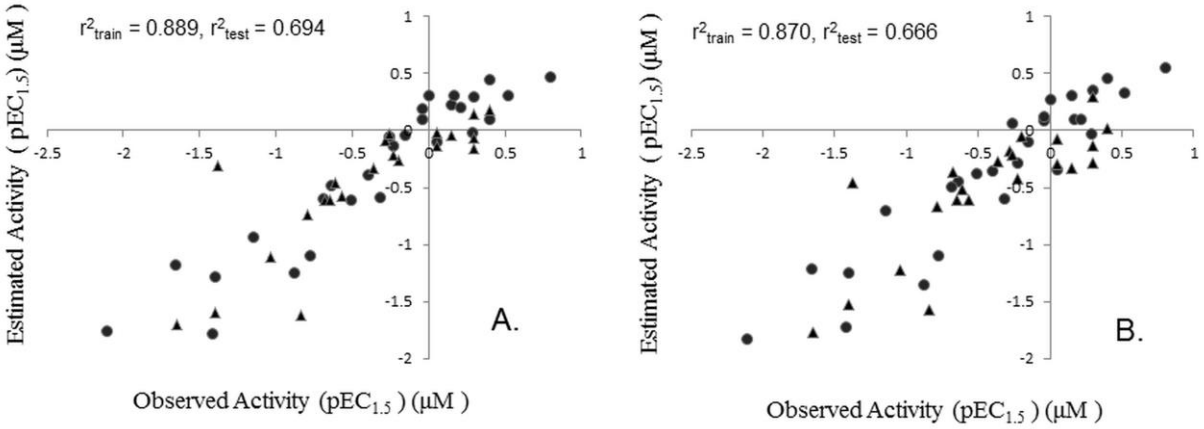

Figure 3. Correlation graph between observed and predicted activities of training set (dots) and test set (triangles) molecules **(A)** CoMFA and **(B)** CoMSIA.

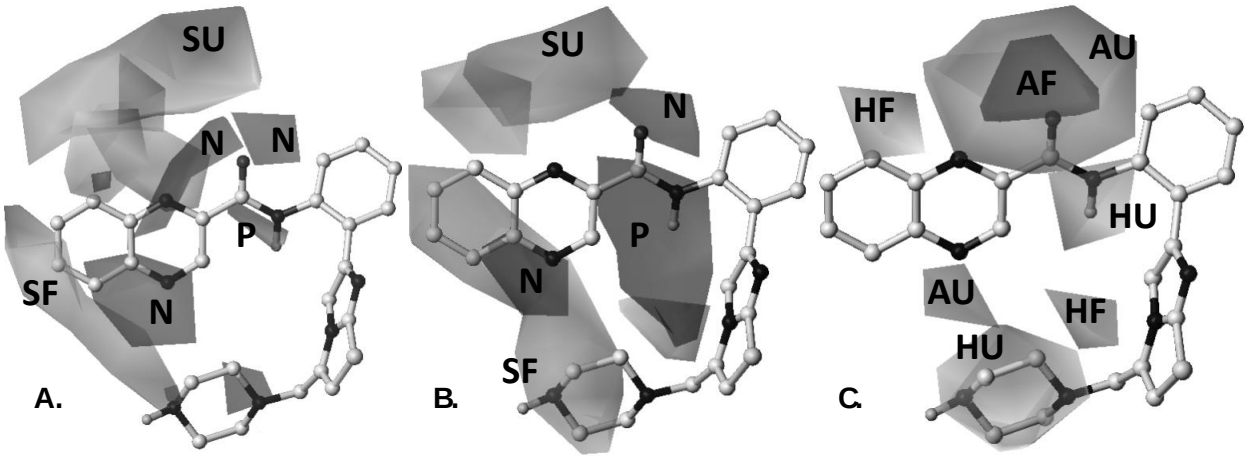

Figure 4. PLS contours from 3D-QSAR analysis of SIRT1 activators **(A)** Steric and electrostatic CoMFA contours; **(B)** Steric and electrostatic CoMSIA contours. The 'SF' and 'SU' labeled contours indicate sterically favored and disfavored regions respectively while the 'P' and 'N' labeled contours denote regions that favor electropositive substituent and electronegative substituent respectively; **(C)** hydrogen bond acceptor and hydrophobic contours. The 'AF' and 'AU' labeled polyhedral represents the favored and disfavored regions respectively for hydrogen bond acceptor feature. Similarly, 'HF' and 'HU' contours represents hydrophobically favored and dis favored regions.

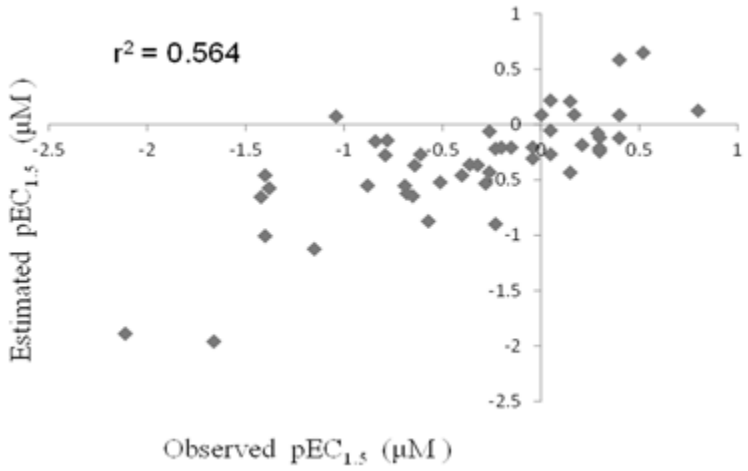

Figure 5. 2D Correlation graph between observed and predicted activities of dataset set ligands.

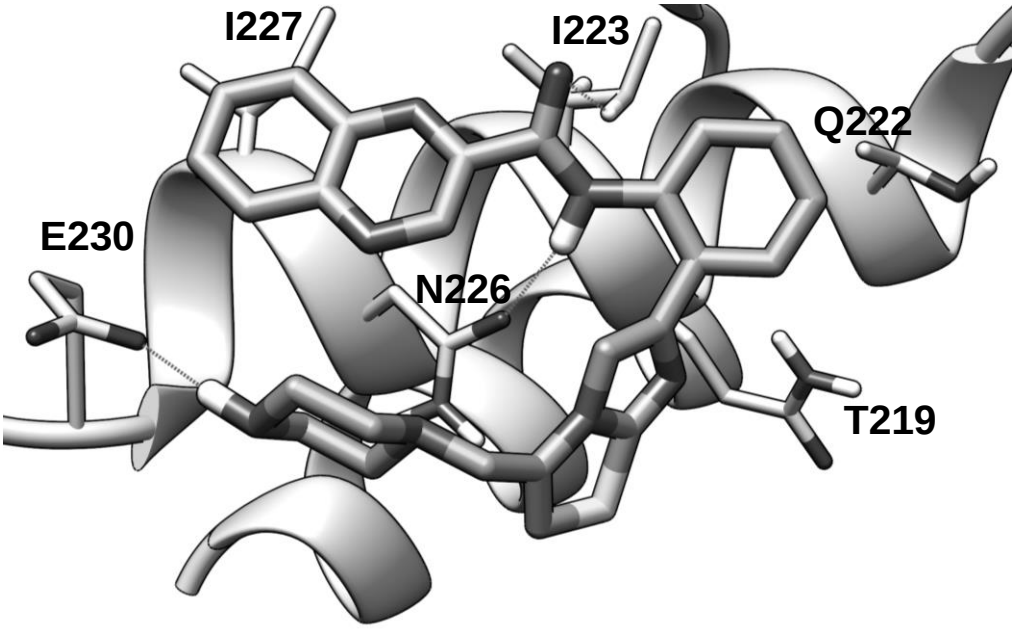

Figure 6. Lowest energy conformation of most active compound **43** bound with active form of SIRT1 protein.